Laboratory Investigation (2018) 98:1211–1224
https://doi.org/10.1038/s41374-018-0078-8

ARTICLE

Thioredoxin-interacting protein deficiency ameliorates kidney inflammation and fibrosis in mice with unilateral ureteral obstruction

Ming Wu[1,2] · Ruoyu Li[1] · Yanjuan Hou[1,3] · Shan Song[1] · Weixia Han[1] · Nan Chen[1] · Yunxia Du[1,2] · Yunzhuo Ren[1,2] · Yonghong Shi[1,2]

Received: 10 August 2017 / Revised: 12 April 2018 / Accepted: 20 April 2018 / Published online: 8 June 2018

Abstract

Thioredoxin-interacting protein (TXNIP) is associated with inflammation, tubulointerstitial fibrosis, and oxidative stress in diabetic kidney disease, yet the potential role of TXNIP in nondiabetic renal injury is not well known. This study aimed to investigate the effect of TXNIP on renal injury by creating a unilateral ureteral obstruction (UUO) model in TXNIP knockout (TKO) mice. We performed sham or UUO surgery in 8-week-old TXNIP KO male mice and age and sex-matched wild-type (WT) mice. Animals were killed at 3, 5, 7, or 14 days after surgery, and renal tissues were obtained for RNA, protein, and other analysis. Our results show that the expression of TXNIP was increased in a time-dependent manner in the ligated kidneys. TXNIP deletion reduced renal fibrosis, apoptosis, α-SMA, TGF-β1 and CTGF expression, and activation of Smad3, p38 MAPK, and ERK1/2 in UUO kidneys. We also found UUO-induced renal F4/80+ macrophage infiltration, MCP-1 expression and activation of NF-κB and NLRP3 inflammasome were attenuated in TKO mice. Furthermore, our study revealed that TXNIP deficiency inhibited the expression of 8-OHdG, heme oxygenase-1 (HO-1) and NADPH oxidase 4 (Nox4) in UUO kidney. In summary, our study suggests that TXNIP plays a key role in the renal inflammation and fibrosis induced by UUO. Inhibition of TXNIP may be a strategy to slow the progression of chronic kidney diseases.

Introduction

Chronic kidney disease (CKD) is a worldwide public health problem. Renal interstitial fibrosis is considered as the final common pathway of virtually all kinds of progressive CKD leading to end-stage renal failure [1, 2]. Renal interstitial fibrosis reflects the imbalance of different mechanisms including renal cells apoptosis, inflammatory cell infiltration, and oxidative stress generation. Oxidative stress has been implicated in the pathogenesis of renal fibrosis in UUO [3, 4]. Prevention of oxidative stress generation has become a therapeutic target to halt the progression of renal injury in UUO [5–7].

Thioredoxin-interacting protein (TXNIP) also known as vitamin D3 up-regulated protein-1(VDUP-1) or thioredoxin-binding protein-2 (TBP-2), is the endogenous inhibitor of cellular thioredoxin (TRX), inactivating its anti-oxidative function by binding to the redox-active cysteine residues [8]. A recent study demonstrated that genetic deletion of TXNIP resulted in reduced oxidative stress, renal fibrosis and extracellular matrix accumulation, podocyte injury and inflammation associated with diabetes [9]. Our previous studies have demonstrated that knockdown of TXNIP reversed high glucose (HG)-induced reduction of TRX activity and inhibited HG-induced ROS production, apoptosis and epithelial-to-mesenchymal transition (EMT) in mesangial cell and HK-2 cell [10, 11]. Knockdown of TXNIP also inhibited TGF-β1-induced ROS generation and EMT in HK-2 cells [11]. TXNIP overexpression resulted in type IV collagen mRNA and protein induction in mesangial

These authors contributed equally: Ming Wu, Ruoyu Li, Yanjuan Hou.

Electronic supplementary material The online version of this article (https://doi.org/10.1038/s41374-018-0078-8) contains supplementary material, which is available to authorized users.

✉ Yonghong Shi
yonghongshi@126.com

[1] Department of Pathology, Hebei Medical University, Shijiazhuang, China

[2] Hebei Key Laboratory of Kidney Diseases, Shijiazhuang, China

[3] Department of Nephrology, Second Hospital, Shanxi Medical University, Taiyuan, China

cells [12]. In addition, TXNIP deletion attenuated oxidative stress, inflammatory cells infiltration, and hepatic fibrosis [13]. However, the role of TXNIP in UUO-induced kidney injury has not been documented.

Recently, it has been shown that nucleotide-binding oligomerization domain-like pyrin domain containing protein 3 (NLRP3) inflammasome contributed to the pathogenesis of renal injuries resulted from diabetes, ischemic, crystal, antineutrophil cytoplasmic antibody, and UUO [14–18]. NLRP3 recruits the apoptosis-associated speck-like protein containing a caspase recruitment domain (ASC) by pyrin domain, and then ASC hydrolyzes procaspase-1. Finally, active caspase-1 cleaves pro-IL-1β and IL-18 into their mature form [19]. IL-1β and IL-18 are cardinal proinflammatory cytokines, which govern the outcome of renal disease [20–22]. A previous study has demonstrated that NLRP3$^{-/-}$ mice had less tubular injury, inflammation, and fibrosis after UUO, associated with a reduction in caspase-1 activation and maturation of IL-1β and IL-18 [18]. Aditionally, there is evidence that TXNIP is essential for activation of the NLRP3 inflammasome and IL-1β production under oxidative stress [23]. In β cells, TXNIP mediates ER stress-induced IL-1β mRNA transcription and IL-1β production by the activation of NLRP3 inflammasome [24]. Palmitate-BSA triggered expression of TXNIP and its interaction with NLRP3, resulting in activation of caspase-1 and IL-1β in human retinal endothelial cells [25]. TXNIP knockdown by siRNA inhibited HG-induced NLRP3 inflammasome activation and IL-1β production in podocyte [26]. Recent publications suggest a physical interaction between TXNIP and NLRP3 [23, 27, 28]. The association of TXNIP with NLRP3 indicates that TXNIP may play a major role in the inflammation that contributes to CKD.

In the present study, we investigated renal expression of TXNIP during the development of renal fibrosis in a UUO model. We used TXNIP knockout (TXNIP$^{-/-}$) mice with UUO to investigate the roles of TXNIP in renal fibrosis, inflammatory cells infiltration, cell apoptosis and NLRP3 inflammasome activation.

Materials and methods

Materials

Antibodies against NLRP3 (sc-66846), ASC (sc-22514-R), caspase-1 p10 (sc-514), fibronectin (sc-6952) and 8-OHdG (sc-66036) were purchased from Santa Cruz Biotechnology (Santa Cruz, CA). NF-κB p65 (ab6502), TXNIP (ab188865), TRX (ab86255), Nox4 (ab218043), HO-1 (ab13243), CTGF (ab6992), MCP-1(ab25124), collagen IV (ab6586), α-SMA (ab5694), Bax (ab32503), Bcl-2 (ab59348), IL-18 (ab71485), α-tubulin (ab7291), histone H3 (ab24834) and F4/80 (ab111101) antibodies were obtained from Abcam (Cambridge, UK). Antibodies for IL-1β (12242), p-Smad3 (9520), Smad3 (9513), ERK1/2 (9102), p-ERK1/2 (9101), cleaved caspase-3 (9664), and caspase-3 (9662) were purchased from Cell Signaling Technology (Beverly, MA). TGF-β1 (18978-1-AP) and β-actin (23660-1-AP) antibodies were obtained from Proteintech (Chicago, IL). TRIzol reagent was obtained from Invitrogen Life Technologies (Carlsbad, CA). Dead End Fluorometric TUNEL System and the reverse transcription system were obtained from Promega (Madison, WI). SYBR Premix Ex TaqTMII was purchased from Takara (Shiga, Japan).

Animals

TXNIP$^{-/-}$ (TXNIP knockout, TKO) mice (C57BL/6J background) were generated by transcription activator-like effector nucleases (TALEN) technique [29]. Wild-type (WT) littermates were used as control. Mice were housed in the animal facilities of Hebei Medical University. The animals underwent left ureteral obstruction or sham operation. Mice were killed and the kidneys were collected for further analysis at 3, 5, 7, and 14 days after surgery. All experimental procedures were approved by the Hebei Medical University Animal Ethics Committee.

Histology and immunohistochemistry

Kidneys were fixed in 4% paraformaldehyde overnight, embedded in paraffin and four-micrometer sections were prepared. Periodic acid-Schiff (PAS) staining was used to evaluate the tubular injury scoring as described previously [30]. Briefly, ten randomly chosen, non-overlapping fields (×400) were examined. Each field was evaluated for tubular injury (tubular dilatation, epithelial simplification, and interstitial expansions). Lesions were graded on a scale from 0 to 4: 0 = normal; 1 = mild, involvement of <25% of the cortex; 2 = moderate, involvement of 25–50% of the cortex; 3 = severe, involvement of 50–75% of the cortex; 4 = involving >75% of the cortex. Sections were stained with Masson's trichrome according to a standard protocol. Then, five fields in the cortex of the kidneys were used. The collagen-positive areas were analyzed using HPIAS-2000 image analysis software (Champion Image Company, Wuhan, China).

Immunohistochemistry for antibodies on renal sections was performed with SP kit according to the instruction. Paraffin-embedded tissue sections were deparaffinized in xylene and rehydrated through graded ethanol. Internal peroxidase was inactivated with 3% hydrogen peroxide in 100% methanol for 30 min. Antigen retrieval was

Table 1 Sequences of the real-time PCR Primers

Genes	Forward primers (5′-3′)	Reverse primers (5′-3′)
TXNIP	CCGTTAGGATCCTGGCTTGC	GGCGCCTTGTACTCATATTTGTTTC
Fibronectin	GAACAGTGGCAGAAAGAATA	CAGGTCTACGGCAGTTGT
Collagen IV	TCGGACCCACTGGTGATAAAG	AAGCCCATTCCTCCAACTGA
NLRP3	TGGGGTACCCTTAGAGGTTTCA	CCTGTTGATCGCAGCAAAGAT
ASC	TCTGGAGTCGTATGGCTTGG	TGCTTGCCTGTGCTGGTC
Caspase-1	CAGGAGGGAATATGTGGG	CACCTTGGGCTTGTCTTT
α-SMA	GAAGAGCATCCGACACTG	GGCATAGCCCTCATAGATAG
MCP-1	GCCTGCTGTTCACAGTTGC	CAGGTGAGTGGGGCGTTA
TGF-β1	GGCGGTGCTCGCTTTGTA	TTTCTCATAGATGGCGTTGTT
CTGF	CACAGAGTGGAGCGCCTG	GATGCACTTTTTGCCCTTCTTAAG
Nox4	CGAGCCAAAGGGGCCCTGAAG	AACAGCGTGCGTCTAACGGCA
HO-1	ATCGTGCTCGCATGAACACT	CCAACACTGCTATTACATGGC
β-actin	GGTACCACCATGTACCCAGG	GAAAGGGTGTAAAACGCAGC

subsequently performed by autoclaving for 15 min at 121 °C in sodium citrate buffer (pH 6.0). After blocking with 10% normal goat serum for 30 min at room temperature, the sections were incubated with primary antibodies for TXNIP, TRX, NLRP3, ASC, caspase-1 p10, TGF-β1, CTGF, F4/80, NF-κB p65, α-SMA, 8-OHdG, Nox4, HO-1, and collagen IV overnight at 4 °C. Sections were then washed and incubated with biotinylated secondary antibody and horseradish peroxidase-conjugated streptavidin. Labeling was visualized with 3,3-diaminobenzidine to produce a brown color, and sections were counterstained with hematoxylin.

TUNEL assay

Investigation of apoptotic cells was performed using terminal deoxynucleotidyl transferase-mediated dUTP nick-end labeling (TUNEL) with Dead End Fluorometric TUNEL System, according to the manufacturer's instructions. The numbers of TUNEL positive apoptotic cells were counted from ten different fields (×400) for each sample and were averaged.

RNA isolation and quantitative real-time PCR

Total RNA was isolated from mouse kidney using TRIzol reagent according to the manufacturer. The cDNA synthesis was performed using M-MLV reverse transcription kit. PCR primers (Table 1) were designed and synthesized from Sangon Biotech Co, Ltd. (Shanghai, China). Real-time PCR was performed in a 96-well optical reaction plate using SYBR Premix Ex TaqTM II. Real-time PCR reactions were performed on Agilent Mx3000P QPCR Systems (Agilent, CA, USA). Relative changes in gene expression were calculated using the $2^{-\triangle\triangle CT}$ method, and all experiments were repeated at least three times.

Protein extraction and Western blotting

Protein from homogenized frozen kidney was prepared in a lysis buffer (Millipore, Billerica, MA) according to the standard procedure. Nuclear and cytoplasmic proteins were extracted from mouse kidneys using a commercial nuclear extraction kit (Active Motif, Carlsbad, CA). Equal amounts of 50 μg total protein were resolved by SDS-PAGE and transferred onto polyvinylidene difluoride membranes (Millipore, Billerica, MA). The membranes were incubated overnight at 4 °C with primary antibodies for TXNIP, TRX, collagen IV, fibronectin, NLRP3, ASC, caspase-1 p10, IL-1β, IL-18, TGF-β1, CTGF, MCP-1, NF-κB p65, Bax, Bcl-2, cleaved caspase-3, caspase-3, Smad3, p-Smad3, p38 MAPK, p-p38 MAPK, ERK1/2, p-ERK1/2, α-SMA, HO-1, and Nox4, respectively. Immunoblots were visualized by the ECL detection system (KPL Mandel Scientific) and then scanned using the Odyssey Fc System (LI-COR, USA). The densitometric analyses were conducted with Image J software (National Institutes of Health).

Statistical analysis

All values are expressed as means ± s.e.m. Statistical analysis was performed by one-way ANOVA, followed by the LSD post hoc *t*-test for multiple comparisons. $P < 0.05$ was considered statistically significant.

Results

Renal TXNIP expression in mouse UUO

Renal TXNIP levels have not been previously examined in UUO. Thus, we determined mRNA levels of TXNIP in mouse kidneys of the different study groups by real-time

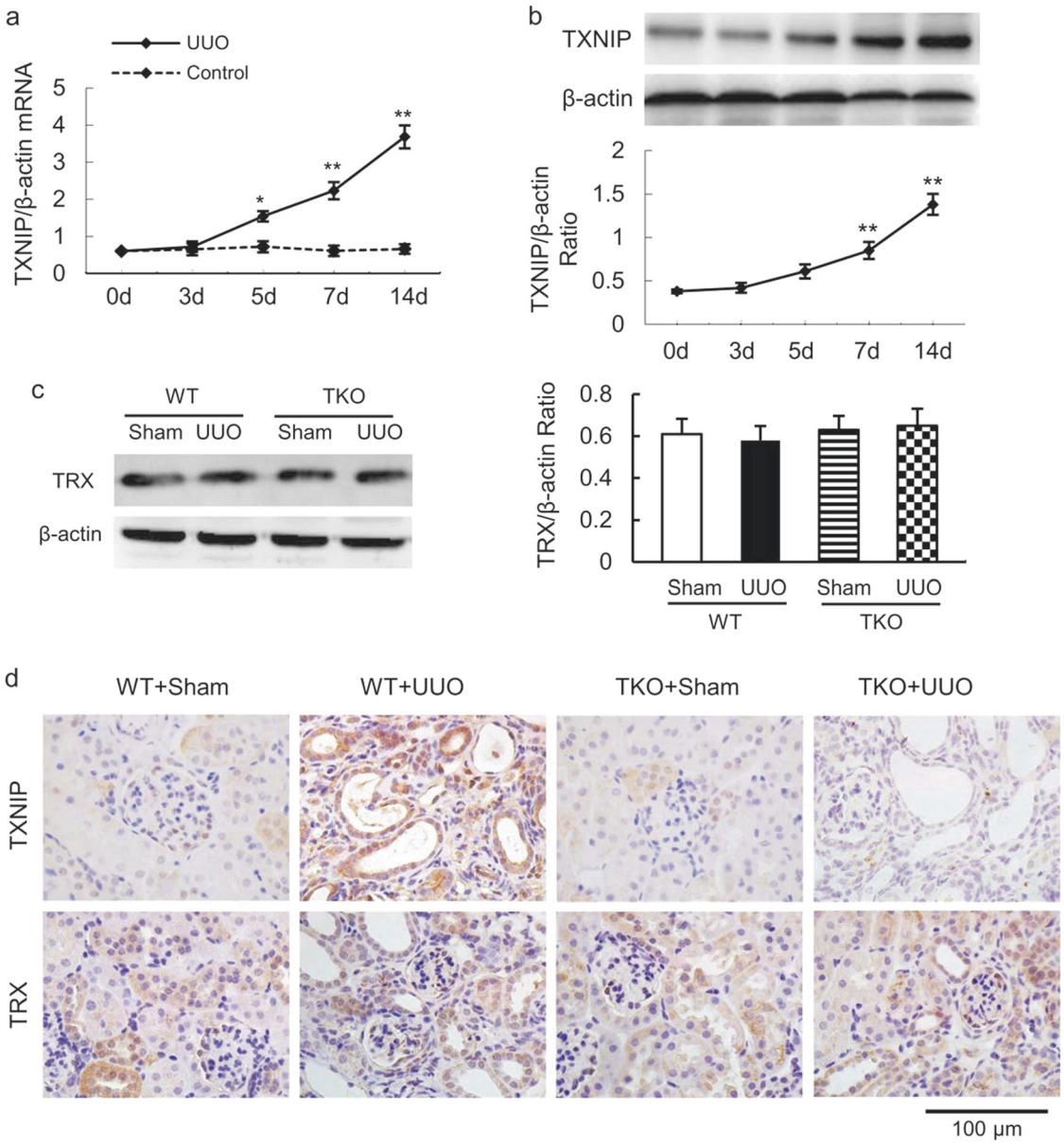

Fig. 1 Renal TXNIP expression after unilateral ureteral obstruction (UUO). TXNIP mRNA (**a**) and protein (**b**) expression of kidney tissue from C57BL/6J mice at 0, 3, 5, 7, and 14 days after UUO were detected by real-time PCR and Western blot. **c** Renal TRX protein level was detected by Western blot. **d** Immunohistochemical staining of TXNIP and TRX in mice kidney tissues. All values are expressed as means ± s.e.m. $N = 6$. $^{*}P < 0.05$, $^{**}P < 0.01$ vs. control group (0 day)

PCR. As shown in Fig. 1a, TXNIP mRNA levels increased in a time-dependent manner. We next examined the protein expression of TXNIP in mouse kidneys by Western blot and immunohistochemistry staining. Consistent with the mRNA expression data, Western blot analysis revealed that UUO induced significantly increase of TXNIP protein expression (Fig. 1b). Immunohistochemistry staining for TXNIP showed weak expression in WT sham mouse kidney (Fig. 1d). Increased expression of TXNIP was found in tubules of WT UUO mice at 14 days after UUO (Fig. 1d). There was no significant difference in TRX protein expression among four groups at 14 days after UUO (Fig. 1c, d).

UUO-induced renal fibrosis is attenuated in TKO mice

To investigate the role of TXNIP in the progression of renal fibrosis, we analyzed tubular injury scores using PAS-stained kidney sections. As shown in Fig. 2a, b, we found that WT mice demonstrated significant tubular injury at 14 days after UUO. However, TKO mice

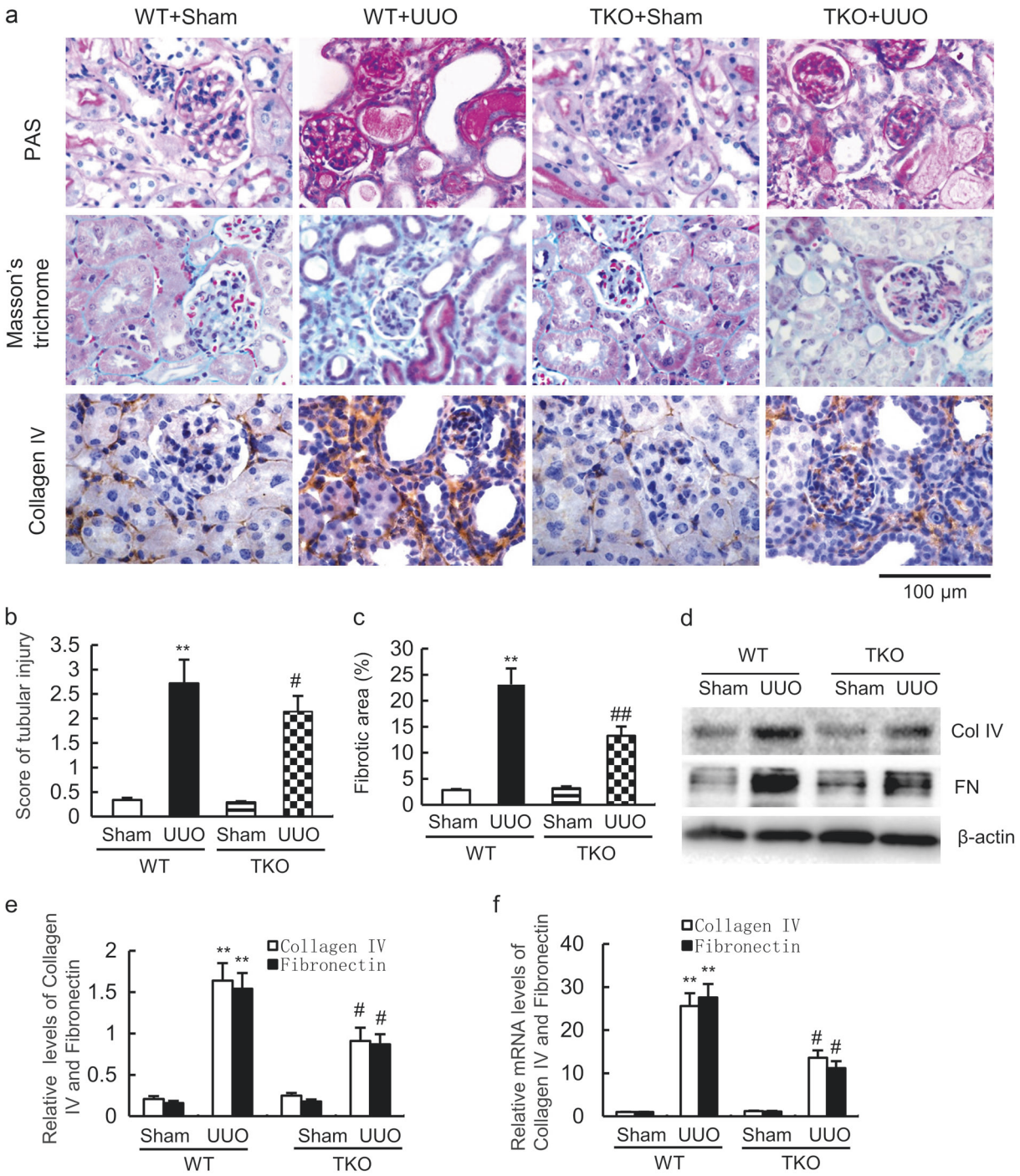

Fig. 2 TXNIP deletion alleviated tubular injury and renal tubulointerstitial collagen deposition after UUO. **a** After 14 days UUO, kidney sections were stained with periodic acid Schiff (PAS), Masson trichrome, and immunohistochemical staining with collagen IV antibody. Tubular injury score (**b**) and fibrotic area (**c**) were measured. **d** Representative Western blots for fibronectin and collagen IV. **e** Semiquantitative analysis of the fibronectin and collagen IV from the Western blot data. **f** Renal mRNA levels of fibronectin and collagen IV were detected by real-time PCR. All values are expressed as means ± s.e.m. $N = 6$. $^{**}P < 0.01$ vs. WT+sham, $^{\#}P < 0.05$ vs. WT + UUO

showed less tubular injury in the obstructed kidneys than WT mice after UUO. Masson's trichrome and quantitative assessment confirmed that TKO mouse kidneys showed a significant reduction in fibrosis at 14 days after UUO compared with WT kidneys (Fig. 2a, c). The expression levels of collagen IV and fibronectin were significantly elevated in the UUO WT group compared with WT sham group. These changes were significantly remitted in TKO mice (Fig. 2a, d, e). Next, we examined the effect of TXNIP on the mRNA expression

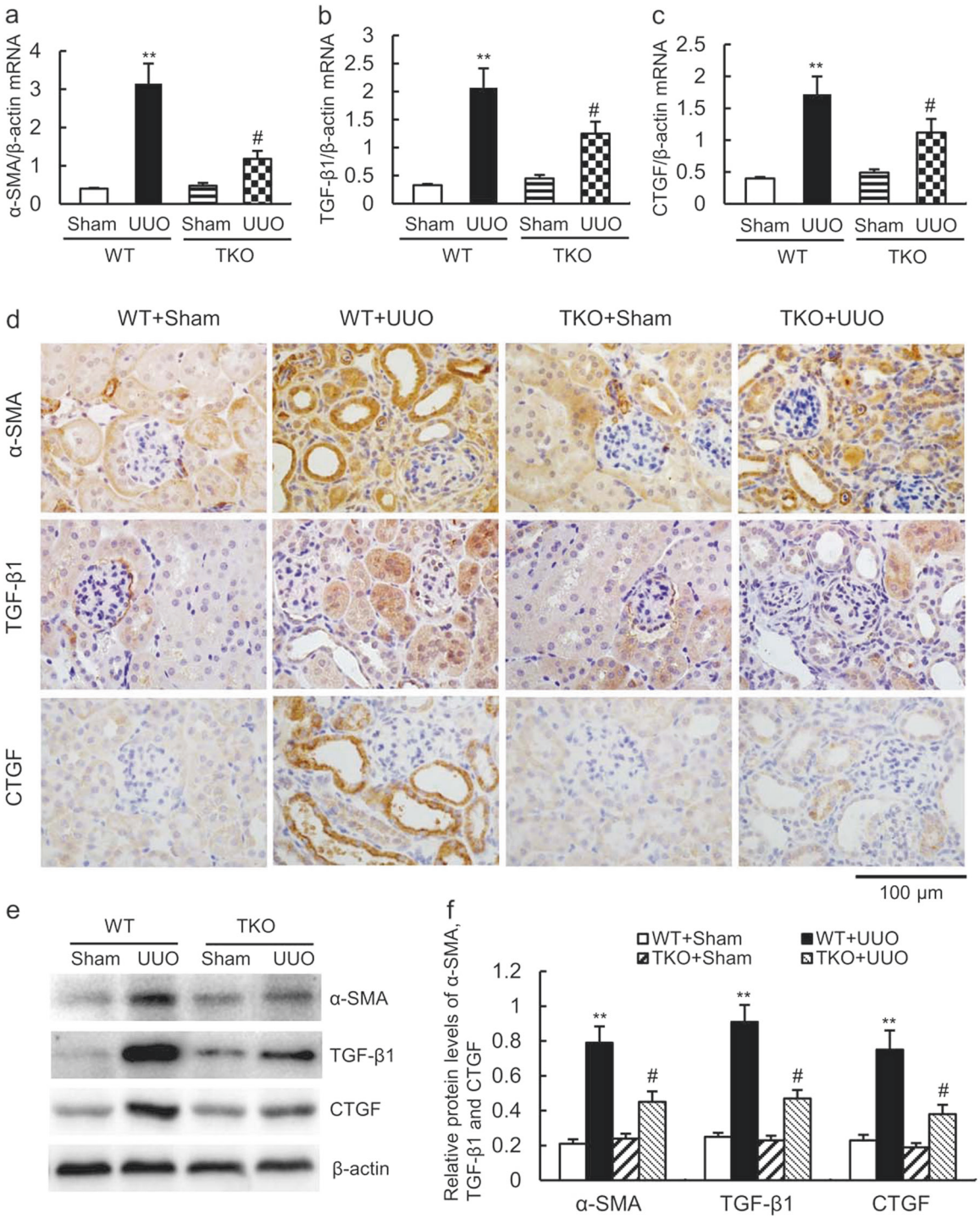

Fig. 3 TXNIP deletion inhibited renal expression of α-SMA, TGF-β1, and CTGF in UUO mice. The mRNA levels of α-SMA (**a**), TGF-β1 (**b**), and CTGF (**c**) in kidney tissue were detected by real-time PCR. **d** Immunohistochemical staining of kidney sections with α-SMA, TGF-β1, and CTGF antibodies. **e** Representative Western blots for α-SMA, TGF-β1, and CTGF. **f** Semiquantitative analysis of the α-SMA, TGF-β1, and CTGF from the Western blot data. All values are expressed as means ± s.e.m. $N = 6$. $^{**}P < 0.01$ vs. WT+sham, $^{\#}P < 0.05$ vs. WT + UUO

of fibronectin and collagen IV. As shown in Fig. 2f, a marked induction of fibronectin and collagen IV mRNA was observed in the kidneys of UUO WT mice compared with sham control. TXNIP deficiency significantly inhibited the mRNA expression of fibronectin and collagen IV in UUO kidney. These results suggest that TXNIP plays an important role in the induction of fibrosis in UUO.

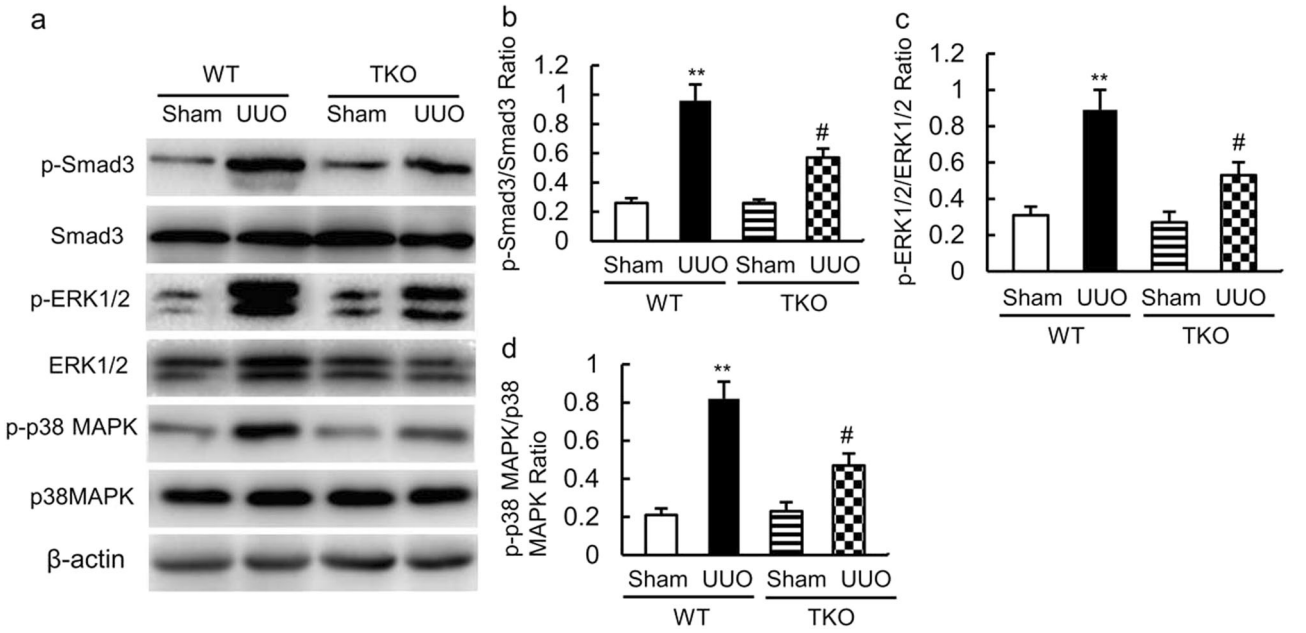

Fig. 4 TXNIP deletion inhibited Smad3, ERK1/2, and p38 MAPK activation in UUO kidney. **a** The expression of p-Smad3, Smad3, p-ERK1/2, ERK1/2, p-p38 MAPK, and p38 MAPK were detected by Western blot. Semiquantitative densitometry analysis of p-Smad3 (**b**), p-ERK1/2 (**c**), and p-p38 MAPK (**d**) from the Western blot data. All values are expressed as means ± s.e.m. $N = 6$. $^{**}P < 0.01$ vs. WT + sham, $^{\#}P < 0.05$ vs. WT + UUO

We next measured the profibrotic gene expression in UUO kidneys for α-SMA, TGF-β1, and CTGF. As shown in Fig. 3a–c, the renal mRNA expression levels of α-SMA, TGF-β1, and CTGF were significantly increased in UUO WT mice compared with WT sham mice. UUO-induced renal mRNA upregulation of α-SMA, TGF-β1, and CTGF was markedly suppressed in the TKO mice. Increased protein expression levels of α-SMA, TGF-β1, and CTGF were observed in the kidneys at 14 days after UUO (Fig. 3d–f). However, the increases in α-SMA, TGF-β1, and CTGF expression were significantly depressed in the TKO kidneys (Fig. 3d–f).

TXNIP deficiency prevents UUO-induced Smad3, p38 MAPK, and ERK1/2 phosphorylation

Because Smad3, p38 MAPK, and ERK1/2 signaling pathways play important role in UUO [4, 31, 32], we determined the phosphorylation levels of Smad3, p38 MAPK, and ERK1/2 in kidneys at 14 days after UUO. As shown in Fig. 4, Western blot showed that the phosphorylation levels of Smad3, p38 MAPK, and ERK1/2 in kidneys were significantly increased in UUO WT mice compared with sham WT mice. The increased phosphorylation levels of Smad3, p38 MAPK, and ERK1/2 were inhibited significantly by TXNIP deficiency. Taken together, these data indicate that TXNIP deficiency reduces renal damage through regulation of Smad3, p38 MAPK, and ERK1/2 phosphorylation in UUO.

TXNIP deletion reduces renal inflammation and NF-κB activation in UUO

To determine whether UUO-induced renal inflammation was associated with TXNIP, we detected F4/80 and MCP-1 expression in UUO mice kidneys. There was an increase in the number of F4/80-positive macrophage infiltration at 14 days after UUO in WT mice (Fig. 5a, b). The increase in F4/80-positive cells was significantly reduced in the TKO kidneys (Fig. 5a, b). Consistent with the reduction in F4/80-positive cells, UUO-induced MCP-1 expression was ameliorated in the kidneys of TKO mice (Fig. 5c, d).

Previous study has shown that nuclear factor κB (NF-κB) activation played an important role in renal injury after UUO [33]. We detected NF-κB p65 expression in UUO kidneys using Western blot and immunohistochemistry staining. At 14 days, TKO mice displayed less NF-κB transfer from cytoplasm to nuclear compared with WT UUO group (Fig. 5a, e, f). These results suggested that TKO mice display obviously reduced renal inflammation and NF-κB activation, which protects against the tubular injury after UUO.

TXNIP deletion inhibits renal NLRP3 inflammasome in UUO

A previous study has shown that activation of the NLRP3-ASC-caspase-1-IL-β axis plays an important role in renal malfunction following UUO [18]. Therefore, we evaluated

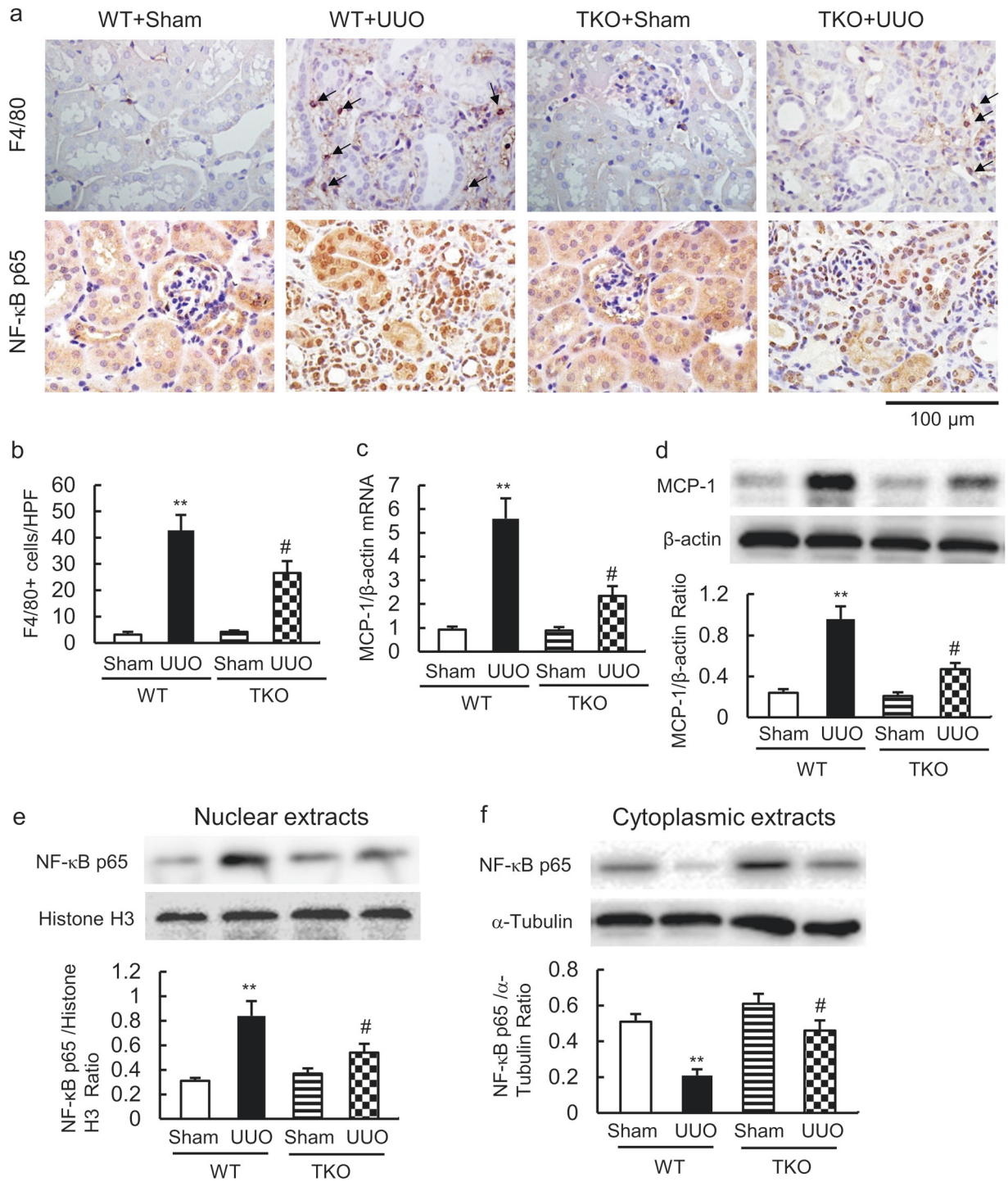

Fig. 5 TXNIP deletion reduced renal inflammation and NF-κB activation in UUO mice. **a** Immunohistochemistry of kidney tissues with F4/80 and NF-κB p65 antibodies. **b** Quantitative analysis of F4/80-positive cells in kidney of UUO mice. Renal MCP-1 mRNA (**c**) and protein (**d**) levels were detected by real-time PCR and Western blot. The expression levels of NF-κB p65 in nuclear extracts (**e**) and cytoplasmic extracts (**f**) were detected by Western blot. All values are expressed as means ± s.e.m. $N = 6$. $^{**}P < 0.01$ vs. WT + sham, $^{\#}P < 0.05$ vs. WT + UUO

the role of TXNIP in activation of NLRP3 inflammasome in UUO kidneys. As shown in Fig. 6a–d, the expression levels of NLRP3, ASC, caspase-1 p10, IL-18, and cleaved IL-1β in UUO kidneys were increased compared with sham group. The increased expression levels of NLRP3, ASC, caspase-1 p10, IL-18, and cleaved IL-1β in UUO kidneys were inhibited significantly by TXNIP deficiency (Fig. 6a–d). Moreover, UUO markedly induced NLRP3,

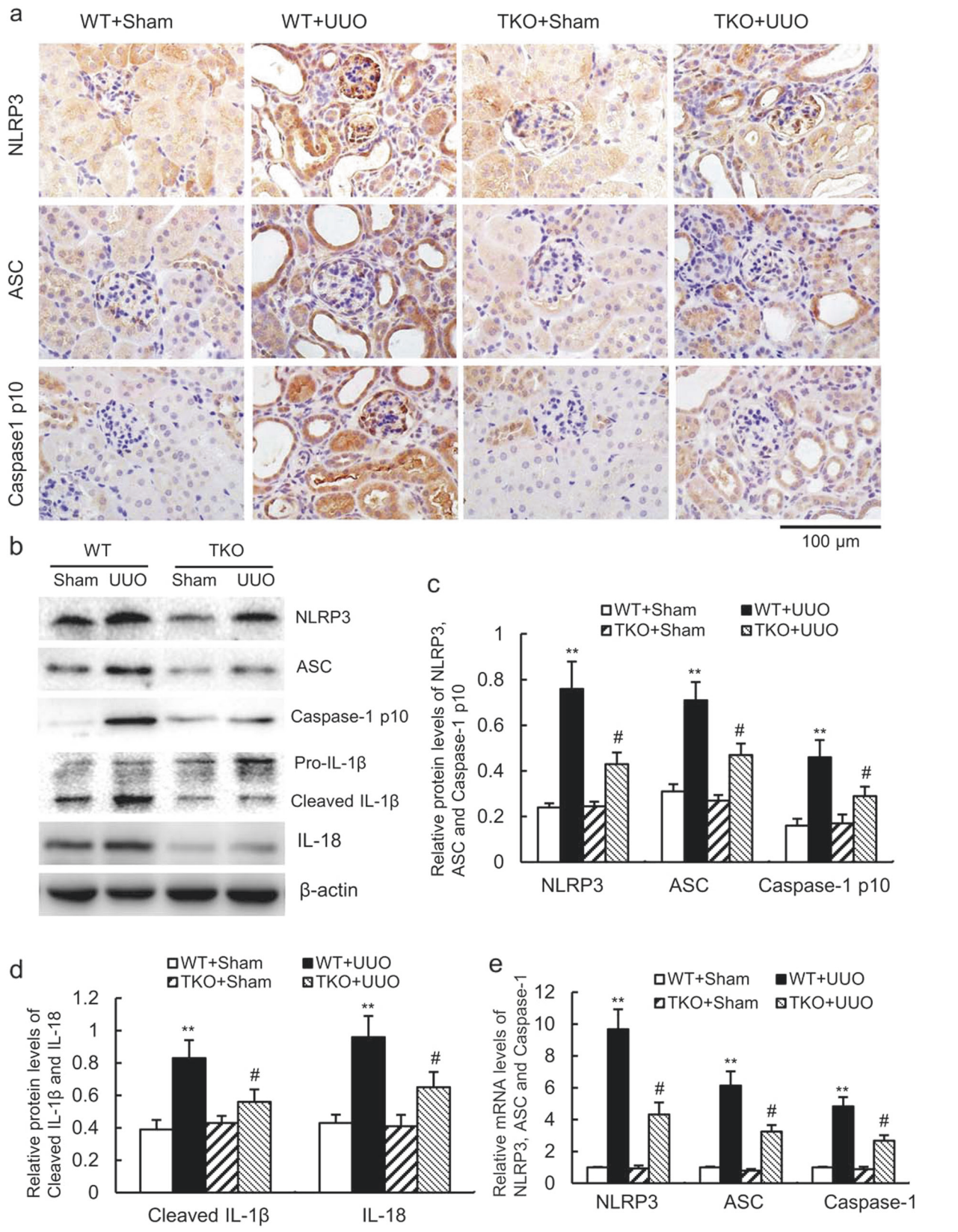
a
WT+Sham
WT+UUO
TKO+Sham
TKO+UUO
NLRP3
ASC
Caspase1 p10
100 μm
b
WT
TKO
Sham
UUO
Sham
UUO
NLRP3
ASC
Caspase-1 p10
Pro-IL-1β
Cleaved IL-1β
IL-18
β-actin
c
WT+Sham
WT+UUO
TKO+Sham
TKO+UUO
Relative protein levels of NLRP3, ASC and Caspase-1 p10
NLRP3
ASC
Caspase-1 p10
d
Relative protein levels of Cleaved IL-1β and IL-18
Cleaved IL-1β
IL-18
e
Relative mRNA levels of NLRP3, ASC and Caspase-1
NLRP3
ASC
Caspase-1

◀ **Fig. 6** TXNIP knockout prevented renal NLRP3 inflammasome activation. **a** Immunohistochemistry of kidney tissues with NLRP3, ASC, and caspase-1 p10 antibodies. **b** Representative Western blots for NLRP3, ASC, and caspase-1 p10, IL-1β, and IL-18. Semiquantitative analysis of the NLRP3, ASC, and caspase-1 p10 (**c**) and cleaved IL-1β and IL-18 (**d**) from the Western blot data. **e** Renal mRNA levels of NLRP3, ASC, and caspase-1 were detected by real-time PCR. All values are expressed as means ± s.e.m. $N = 6$. $^{**}P < 0.01$ vs. WT + sham, $^{\#}P < 0.05$ vs. WT + UUO

ASC, and caspase-1 mRNA expression in WT kidneys. However, the induction of NLRP3, ASC, and caspase-1 mRNA expression by UUO was significantly prevented by TXNIP deletion (Fig. 6e).

TXNIP deletion suppresses renal apoptosis in UUO

We next investigated whether TXNIP knockout affected UUO-induced apoptosis in the kidneys. By TUNEL assay, apoptosis was seen predominantly in the renal tubular cells of mice at 14 days after UUO (Fig. 7a, b). UUO-induced apoptosis was attenuated significantly by TXNIP deletion (Fig. 7a, b). Increased apoptosis in UUO kidneys was further confirmed by higher levels of cleaved caspase-3 expression comparing with the sham group, and TXNIP deletion significantly reduced UUO-induced increase of cleaved caspase-3 (Fig. 7c, d). Furthermore, we observed the effect of TXNIP deficiency on expression of Bax and Bcl-2 in UUO kidneys. Bax expression was increased and Bcl-2 expression was decreased in kidneys from the WT UUO group compared with WT sham group, and these changes were significantly reversed by TXNIP deficiency (Fig. 7c, e, f). These results suggest that TXNIP deficiency protects the kidney from renal cell apoptosis of UUO.

TXNIP deletion attenuates UUO-induced oxidative stress

Oxidative stress is believed to be an important mediator in the development of renal fibrosis [6, 34]. Therefore, we investigated the effect of TXNIP on UUO-induced oxidative stress. We first examined the expression of 8-OHdG by immunohistochemistry. The expression of 8-OHdG was significantly increased in WT UUO kidneys compared with WT sham group (Fig. 8a). TXNIP deletion reduced UUO-induced 8-OHdG expression (Fig. 8a). Next, we evaluated the effect of TXNIP deletion on Nox4 and HO-1 expression after UUO. The expression levels of Nox4 and HO-1 were significantly increased in kidneys at 14 days after UUO (Fig. 8a–d). The UUO-induced renal Nox4 and HO-1 expression was reduced in TKO mice (Fig. 8a–d). Furthermore, the UUO-induced Nox4 and HO-1 mRNA expression levels were also alleviated by TXNIP deletion (Fig. 8e, f).

Discussion

In this study, we found that the mRNA and protein expression of TXNIP was significantly upregulated in kidneys after UUO. TXNIP deficiency inhibited the increase in renal fibrosis, inflammatory cells infiltration, and cell apoptosis in UUO mice. TXNIP deletion reduced renal expression of α-SMA, TGF-β1, and CTGF, and activation of Smad3, p38 MAPK, and ERK1/2 in UUO mice. UUO-induced renal MCP-1 expression and activation of NF-κB and NLRP3 inflammasome were attenuated in TXNIP KO mice. Furthermore, TXNIP deficiency inhibited the expression of 8-OHdG, HO-1, and Nox4 in UUO kidney. These results indicate that inhibition of TXNIP protected against the progression of renal interstitial fibrosis.

The expression of TXNIP markedly upregulated in diabetic kidney, and which has been suggested to play a role in diabetic nephropathy [9, 35]. Previous studies have demonstrated that transcription factors Krüppel-like factor 6 (KLF6), peroxisome proliferator-activated receptor-γ (PPAR-γ) and epigenetic regulation were involved in regulation of TXNIP in diabetic kidney [36, 37]. It has been reported that KLF6 was dramatically increased in UUO kidney [38]. PPAR-γ activity was reduced by UUO and PPAR-γ agonist could attenuate renal interstitial fibrosis and inflammation in UUO mice [39, 40]. Taken together, these data suggest that the expression of TXNIP may be mediated by KLF6 and PPAR-γ in UUO kidney.

Previous studies have shown that oxidative stress contributed importantly to the pathogenesis of UUO [3, 4]. Increased renal concentrations of reactive oxygen species (ROS) have been observed in obstructed kidneys [34]. NAD(P)H oxidase-derived generation of superoxide is recognized as an important mediator of renal fibrosis [4, 41]. Several studies demonstrated a crucial role for Nox4 as the source of ROS in kidneys after UUO [5, 42]. It has been reported that TXNIP mediated HG-induced ROS generation by mitochondrial and Nox4 in mesangial cells [43]. Moreover, TXNIP deficiency inhibited renal oxidative stress and NOX4 expression in diabetic mice [9]. In this study, we found that TXNIP mRNA and protein expression levels were increased in kidneys after UUO. TXNIP knockout significantly alleviated UUO-induced 8-OHdG, HO-1, and Nox4 expression. Therefore, our findings suggest that TXNIP is involved in ROS generation in kidneys after UUO.

There is accumulating evidence that TXNIP plays a pivotal role in renal fibrosis associated with diabetes. Overexpression of TXNIP resulted in increased tissue collagen accumulation in association with the development of matrix accumulation and fibrosis in diabetic nephropathy [12]. Knockdown of TXNIP resulted in attenuation of high glucose-induced 3H-proline incorporation in mesangial

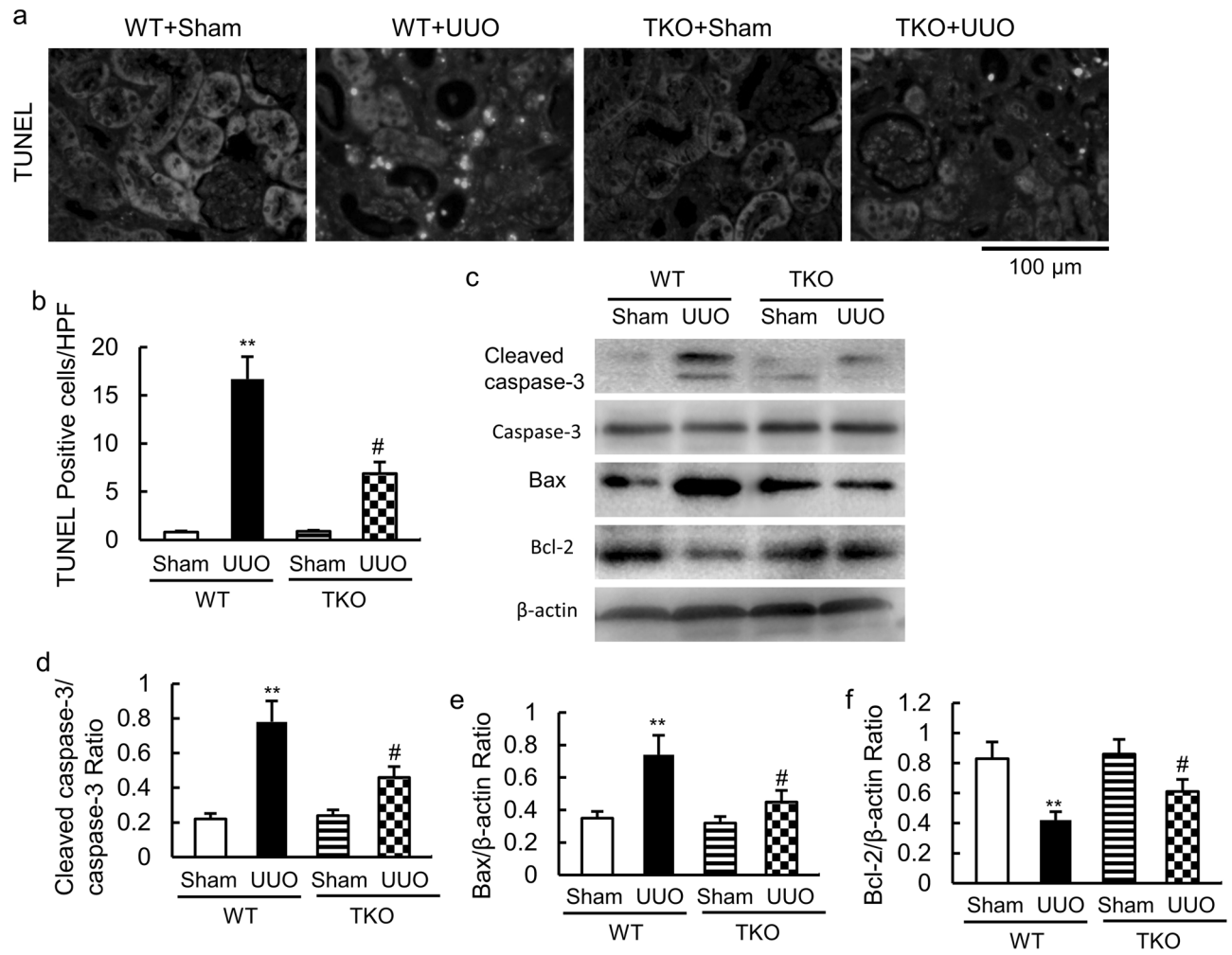

Fig. 7 TXNIP knockout attenuated renal cell apoptosis in UUO mice. **a** Apoptosis was assessed by TUNEL. **b** Apoptotic cells per field. **c** The expression levels of cleaved caspase-3, Bax, and Bcl-2 were detected by Western blot analysis. **d** The relative intensity of cleaved caspase-3 was normalized to the caspase-3. The relative intensity of Bax (**e**) and Bcl-2 (**f**) were normalized against β-actin. All values are expressed as means ± s.e.m. $N = 6$. $^{**}P < 0.01$ vs. WT + sham, $^{\#}P < 0.05$ vs. WT + UUO

cells and proximal tubules cells [35]. Our group demonstrated that knockdown of TXNIP prevented HG or TGF-β1-induced α-SMA expression in HK-2 cells [11]. Diabetes-induced matrix accumulation and fibrosis in the kidneys were prevented by TXNIP deletion [9]. In this study, we found that enhanced fibrosis was associated with significantly increased expression of TXNIP in kidneys after UUO. TXNIP KO alleviated UUO-induced tubular injury, renal fibrosis, and profibrotic genes (α-SMA, TGF-β1, and CTGF) expression in mice. Taken together, these data suggest that TXNIP plays a role in pathogenesis of renal fibrosis.

Inflammatory cell infiltration plays a key role in the onset and progression of renal injury after UUO [44, 45]. Previous study demonstrated that TXNIP is mediated with vascular inflammation under disturbed-flow [46]. Diabetes-induced renal inflammation was prevented by TXNIP deletion [9]. In our present study, obstructed kidneys of WT mice presented a marked interstitial inflammatory cell infiltration and increased inflammation cytokine MCP-1 expression at 14 days after UUO, whereas obstructed kidneys of TXNIP KO mice showed decreased interstitial inflammatory cell infiltration and MCP-1 expression. Taken together, TXNIP deficiency alleviates UUO-induced renal injury by suppression of inflammation.

The NLRP3 inflammasome is an innate proteolytic complex that is known to be activated by a variety of nonmicrobial danger signals. Previous study has shown that NLRP3 inflammasome was activated in kidneys after UUO, and UUO-induced tubular injury, inflammation, and fibrosis were ameliorated in NLRP3$^{-/-}$ or ASC$^{-/-}$ mice [47]. It has been reported that TXNIP as a binding partner to NLRP3, where association between these two proteins was necessary for downstream inflammasome activation [23]. Inhibition of TXNIP prevented TXNIP-NLRP3 binding and subsequent NLRP3 inflammasome

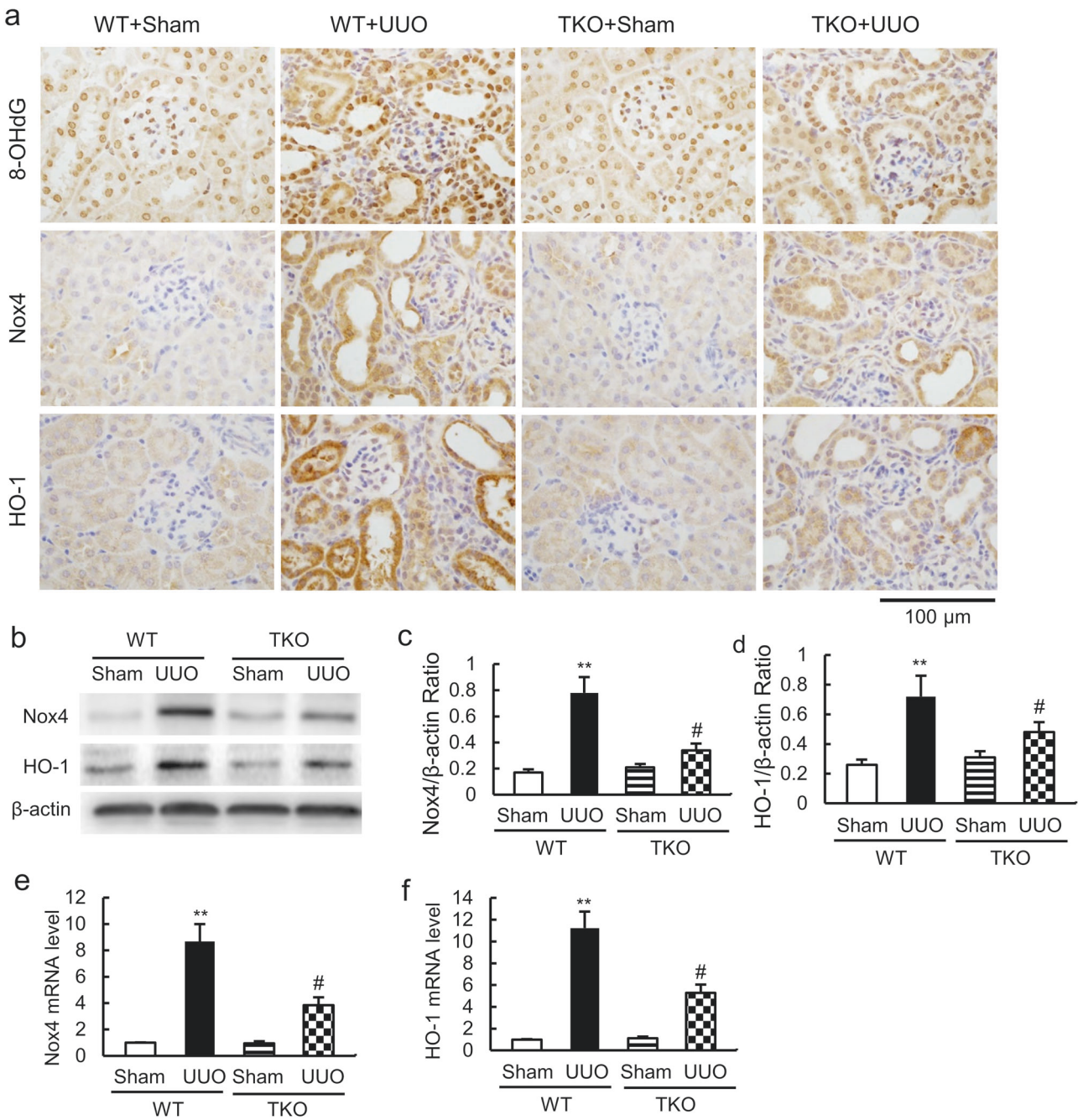

Fig. 8 Renal oxidative stress was reduced in TXNIP KO mice after UUO. **a** Immunohistochemistry of kidney tissues with 8-OHdG, Nox4, and HO-1 antibodies. **b** Representative Western blots for Nox4 and HO-1. Semiquantitative analysis of the Nox4 (**c**) and HO-1 (**d**) from the Western blot data. Renal mRNA levels of Nox4 (**e**) and HO-1 (**f**) were detected by real-time PCR. All values are expressed as means ± s.e.m. $N = 6$. $^{**}P < 0.01$ vs. WT + sham, $^{\#}P < 0.05$ vs. WT + UUO

activation in podocyte and glomerular injury during hyperhomocysteinemia [48]. Furthermore, TXNIP could induce IL-1β production through the activation of NLRP3 inflammasome and IL-1β mRNA transcription in β cell [24]. In this study, we found that NLRP3 inflammasome is activated in kidneys after UUO, and UUO-induced renal NLRP3 inflammasome activation was attenuated in TKO mice. TXNIP has been confirmed to be a critical signaling molecule linking oxidative stress to NLRP3 inflammasome activation in a ROS-sensitive manner [49]. In this study, we found that TXNIP deletion inhibited the expression of 8-OHdG, HO-1, and Nox4 in kidney after UUO. Our previous study has shown that knockdown of TXNIP prevented TGF-β1-induced ROS generation in HK-2 cells [11]. Taken together, these results suggest that TXNIP deficiency attenuates UUO-induced renal injury

via inhibition of NLRP3 inflammasome activation mediated by ROS generation.

It has been suggested that renal tubular apoptosis is related to renal tissue loss and dysfunction in UUO [50]. Previous studies have shown that TXNIP contributed to the beta-cell, mesangial cell, and podocyte apoptosis under high glucose conditions [9, 10, 51]. In this study, tubular cell apoptosis was enhanced in kidneys at 14 days after UUO, whereas it was inhibited by TXNIP KO. Furthermore, we evaluated the effect of TXNIP on cleaved caspase-3 expression in UUO kidneys. In accordance with the apoptosis, the expression of cleaved caspase-3 was markedly down-regulated in TXNIP KO mice. In addition, we also found TXNIP KO inhibited Bax expression and reversed reduction of Bcl-2 expression in UUO kidneys. These data suggest that TXNIP deletion protects renal tubular cells from apoptosis after UUO injury.

Multiple intracellular signaling pathways are thought to be involved in kidney injury after UUO, including TGF-β/Smad3, p38 MAPK, and ERK1/2 [4, 31, 32]. Our recent study has demonstrated that knockdown of TXNIP inhibited high glucose-induced TGF-β1 expression, p38 MAPK, and ERK1/2 activation in tubular epithelial cells [11]. In this study, we found that UUO-induced TGF-β1 expression and activation of Smad3, p38 MAPK, and ERK1/2 significantly decreased in TXNIP knockout mice, suggesting that attenuation of TGF-β/Smad3, p38 MAPK, and ERK1/2 signaling pathways in UUO kidney by TXNIP deficiency may be one of the downstream mechanisms underlying protection.

In summary, to our knowledge this is the first in vivo study of UUO in TXNIP-knockout mice. We demonstrate that TXNIP deficient mice showed significant protection from renal injury in UUO models. The reduction in oxidative stress, interstitial inflammation, fibrosis, NLRP3 inflammasome activity, and tubular cell apoptosis is an important reflection of the ability of TXNIP to mediate tissue injury in this model. Our results identify TXNIP as a potential therapeutic target for renal fibrosis-associated kidney diseases.

Acknowledgements This study was supported by grants from the National Natural Science Foundation of China (NO. 81470966 and NO. 81270804), China Postdoctoral Science Foundation funded project (2014M561199) and Hebei Science and Technology Department Program (14277712D).

Compliance with ethical standards

Conflict of interest The authors declare that they have no conflict of interest.

References

1. Zeisberg M, Neilson EG. Mechanisms of tubulointerstitial fibrosis. J Am Soc Nephrol. 2010;21:1819–34.
2. Boor P, Ostendorf T, Floege J. Renal fibrosis: novel insights into mechanisms and therapeutic targets. Nat Rev Nephrol. 2010;6:643–56.
3. Kawada N, Moriyama T, Ando A, et al. Increased oxidative stress in mouse kidneys with unilateral ureteral obstruction. Kidney Int. 1999;56:1004–13.
4. Pat B, Yang T, Kong C, et al. Activation of ERK in renal fibrosis after unilateral ureteral obstruction: modulation by antioxidants. Kidney Int. 2005;67:931–43.
5. Zhou B, Mu J, Gong Y, et al. Brd4 inhibition attenuates unilateral ureteral obstruction-induced fibrosis by blocking TGF-beta-mediated Nox4 expression. Redox Biol. 2017;11:390–402.
6. Jung KJ, Min KJ, Park JW, et al. Carnosic acid attenuates unilateral ureteral obstruction-induced kidney fibrosis via inhibition of Akt-mediated Nox4 expression. Free Radic Biol Med. 2016;97:50–7.
7. Mizuguchi Y, Chen J, Seshan SV, et al. A novel cell-permeable antioxidant peptide decreases renal tubular apoptosis and damage in unilateral ureteral obstruction. Am J Physiol Ren Physiol. 2008;295:F1545–53.
8. Nishiyama A, Matsui M, Iwata S, et al. Identification of thioredoxin-binding protein-2/vitamin D(3) up-regulated protein 1 as a negative regulator of thioredoxin function and expression. J Biol Chem. 1999;274:21645–50.
9. Shah A, Xia L, Masson EA, et al. Thioredoxin-interacting protein deficiency protects against diabetic nephropathy. J Am Soc Nephrol. 2015;26:2963–77.
10. Shi Y, Ren Y, Zhao L, et al. Knockdown of thioredoxin interacting protein attenuates high glucose-induced apoptosis and activation of ASK1 in mouse mesangial cells. FEBS Lett. 2011;585:1789–95.
11. Wei J, Shi Y, Hou Y, et al. Knockdown of thioredoxin-interacting protein ameliorates high glucose-induced epithelial to mesenchymal transition in renal tubular epithelial cells. Cell Signal. 2013;25:2788–96.
12. Kobayashi T, Uehara S, Ikeda T, et al. Vitamin D3 up-regulated protein-1 regulates collagen expression in mesangial cells. Kidney Int. 2003;64:1632–42.
13. Ahsan MK, Okuyama H, Hoshino Y, et al. Thioredoxin-binding protein-2 deficiency enhances methionine-choline deficient diet-induced hepatic steatosis but inhibits steatohepatitis in mice. Antioxid Redox Signal. 2009;11:2573–84.
14. Shahzad K, Bock F, Dong W, et al. Nlrp3-inflammasome activation in non-myeloid-derived cells aggravates diabetic nephropathy. Kidney Int. 2015;87:74–84.
15. Kim HJ, Lee DW, Ravichandran K, et al. NLRP3 inflammasome knockout mice are protected against ischemic but not cisplatin-induced acute kidney injury. J Pharmacol Exp Ther. 2013;346:465–72.
16. Ludwig-Portugall I, Bartok E, Dhana E, et al. An NLRP3-specific inflammasome inhibitor attenuates crystal-induced kidney fibrosis in mice. Kidney Int. 2016;90:525–39.
17. Schreiber A, Luft FC, Kettritz R. Phagocyte NADPH oxidase restrains the inflammasome in ANCA-induced GN. J Am Soc Nephrol. 2015;26:411–24.
18. Vilaysane A, Chun J, Seamone ME, et al. The NLRP3 inflammasome promotes renal inflammation and contributes to CKD. J Am Soc Nephrol. 2010;21:1732–44.
19. Schroder K, Zhou R, Tschopp J. The NLRP3 inflammasome: a sensor for metabolic danger? Science. 2010;327:296–300.
20. Abais JM, Zhang C, Xia M, et al. NADPH oxidase-mediated triggering of inflammasome activation in mouse podocytes and glomeruli during hyperhomocysteinemia. Antioxid Redox Signal. 2013;18:1537–48.

21. Niemir ZI, Stein H, Dworacki G, et al. Podocytes are the major source of IL-1 alpha and IL-1 beta in human glomerulonephritides. Kidney Int. 1997;52:393–403.
22. Szeto HH, Liu S, Soong Y, et al. Mitochondria protection after acute ischemia prevents prolonged upregulation of IL-1beta and IL-18 and arrests CKD. J Am Soc Nephrol. 2017;28:1437–49.
23. Zhou R, Tardivel A, Thorens B, et al. Thioredoxin-interacting protein links oxidative stress to inflammasome activation. Nat Immunol. 2010;11:136–40.
24. Oslowski CM, Hara T, O'Sullivan-Murphy B, et al. Thioredoxin-interacting protein mediates ER stress-induced beta cell death through initiation of the inflammasome. Cell Metab. 2012;16:265–73.
25. Mohamed IN, Hafez SS, Fairaq A, et al. Thioredoxin-interacting protein is required for endothelial NLRP3 inflammasome activation and cell death in a rat model of high-fat diet. Diabetologia. 2014;57:413–23.
26. Gao P, Meng XF, Su H, et al. Thioredoxin-interacting protein mediates NALP3 inflammasome activation in podocytes during diabetic nephropathy. Biochim Biophys Acta. 2014;1843:2448–60.
27. Tseng HH, Vong CT, Kwan YW, et al. TRPM2 regulates TXNIP-mediated NLRP3 inflammasome activation via interaction with p47 phox under high glucose in human monocytic cells. Sci Rep. 2016;6:35016.
28. Xiao YD, Huang YY, Wang HX, et al. Thioredoxin-interacting protein mediates NLRP3 inflammasome activation involved in the susceptibility to ischemic acute kidney injury in diabetes. Oxid Med Cell Longev. 2016;2016:2386068.
29. Zhang H, Liu C, Ma Y, Xiao L, et al. [Efficient preparation of a TXNIP knockout mouse model by transcription activator-like effector nucleases (TALEN)]. Chin J Comp Med. 2015;25:9–13.
30. Jin Y, Liu R, Xie J, et al. Interleukin-10 deficiency aggravates kidney inflammation and fibrosis in the unilateral ureteral obstruction mouse model. Lab Invest. 2013;93:801–11.
31. Sato M, Muragaki Y, Saika S, et al. Targeted disruption of TGF-beta1/Smad3 signaling protects against renal tubulointerstitial fibrosis induced by unilateral ureteral obstruction. J Clin Invest. 2003;112:1486–94.
32. Stambe C, Atkins RC, Tesch GH, et al. The role of p38alpha mitogen-activated protein kinase activation in renal fibrosis. J Am Soc Nephrol. 2004;15:370–9.
33. Tashiro K, Tamada S, Kuwabara N, et al. Attenuation of renal fibrosis by proteasome inhibition in rat obstructive nephropathy: possible role of nuclear factor kappaB. Int J Mol Med. 2003;12:587–92.
34. Manucha W, Carrizo L, Ruete C, et al. Angiotensin II type I antagonist on oxidative stress and heat shock protein 70 (HSP 70) expression in obstructive nephropathy. Cell Mol Biol (Noisy-Le-Grand). 2005;51:547–55.
35. Advani A, Gilbert RE, Thai K, et al. Expression, localization, and function of the thioredoxin system in diabetic nephropathy. J Am Soc Nephrol. 2009;20:730–41.
36. Qi W, Chen X, Holian J, et al. Transcription factors Krüppel-like factor 6 and peroxisome proliferator-activated receptor-{gamma} mediate high glucose-induced thioredoxin-interacting protein. Am J Pathol. 2009;175:1858–67.
37. De Marinis Y, Cai M, Bompada P, et al. Epigenetic regulation of the thioredoxin-interacting protein (TXNIP) gene by hyperglycemia in kidney. Kidney Int. 2016;89:342–53.
38. Karagianni F, Prakoura N, Kaltsa G, et al. Transgelin Up-regulation in obstructive nephropathy. PLOS One. 2013;8:e66887.
39. Kim J, Yoon SP, Toews ML, et al. Pharmacological inhibition of soluble epoxide hydrolase prevents renal interstitial fibrogenesis in obstructive nephropathy. Am J Physiol Ren Physiol. 2015;308: F131–39.
40. Kawai T, Masaki T, Doi S, et al. PPAR-gamma agonist attenuates renal interstitial fibrosis and inflammation through reduction of TGF-beta. Lab Invest. 2009;89:47–58.
41. Barnes JL, Gorin Y. Myofibroblast differentiation during fibrosis: role of NAD(P)H oxidases. Kidney Int. 2011;79:944–56.
42. Xu Y, Ruan S, Wu X, et al. Autophagy and apoptosis in tubular cells following unilateral ureteral obstruction are associated with mitochondrial oxidative stress. Int J Mol Med. 2013;31:628–36.
43. Shah A, Xia L, Goldberg H, et al. Thioredoxin-interacting protein mediates high glucose-induced reactive oxygen species generation by mitochondria and the NADPH oxidase, Nox4, in mesangial cells. J Biol Chem. 2013;288:6835–48.
44. Lange-Sperandio B, Trautmann A, Eickelberg O, et al. Leukocytes induce epithelial to mesenchymal transition after unilateral ureteral obstruction in neonatal mice. Am J Pathol. 2007;171:861–71.
45. Klahr S, Morrissey J. Obstructive nephropathy and renal fibrosis. Am J Physiol Ren Physiol. 2002;283:F861–75.
46. Wang XQ, Nigro P, World C, et al. Thioredoxin interacting protein promotes endothelial cell inflammation in response to disturbed flow by increasing leukocyte adhesion and repressing Kruppel-like factor 2. Circ Res. 2012;110:560–8.
47. Komada T, Usui F, Shirasuna K, et al. ASC in renal collecting duct epithelial cells contributes to inflammation and injury after unilateral ureteral obstruction. Am J Pathol. 2014;184: 1287–98.
48. Abais JM, Xia M, Li G, et al. Nod-like receptor protein 3 (NLRP3) inflammasome activation and podocyte injury via thioredoxin-interacting protein (TXNIP) during hyperhomocysteinemia. J Biol Chem. 2014;289:27159–68.
49. Kim SJ, Lee SM. NLRP3 inflammasome activation in D-galactosamine and lipopolysaccharide-induced acute liver failure: role of heme oxygenase-1. Free Radic Biol Med. 2013;65:997–1004.
50. Truong LD, Petrusevska G, Yang G, et al. Cell apoptosis and proliferation in experimental chronic obstructive uropathy. Kidney Int. 1996;50:200–7.
51. Chen J, Saxena G, Mungrue IN, et al. Thioredoxin-interacting protein: a critical link between glucose toxicity and beta-cell apoptosis. Diabetes. 2008;57:938–44.